Computational and Structural Biotechnology Journal 19 (2021) 5392–5405

COMPUTATIONAL AND STRUCTURAL BIOTECHNOLOGY JOURNAL

journal homepage: www.elsevier.com/locate/csbj

Integrative structural biology of the penicillin-binding protein-1 from *Staphylococcus aureus*, an essential component of the divisome machinery

Siseth Martínez-Caballero [a,2,1], Kiran V. Mahasenan [b,2], Choon Kim [b], Rafael Molina [a], Rhona Feltzer [b], Mijoon Lee [b], Renee Bouley [b], Dusan Hesek [b], Jed F. Fisher [b], Inés G. Muñoz [c], Mayland Chang [b], Shahriar Mobashery [b,*], Juan A. Hermoso [a,*]

[a] Department of Crystallography and Structural Biology, Institute of Physical Chemistry "Rocasolano", CSIC, 28006 Madrid, Spain
[b] Department of Chemistry and Biochemistry, University of Notre Dame, Notre Dame, IN 46556, USA
[c] Structural Biology Programme, Spanish National Cancer Research Center (CNIO), 28029 Madrid, Spain

ARTICLE INFO

Article history:
Received 22 June 2021
Received in revised form 13 September 2021
Accepted 15 September 2021
Available online 17 September 2021

Keywords:
Divisome
Staphylococcus aureus
X-ray crystal structure
SAXS in-solution structure
Molecular dynamics simulations
PBP1
PASTA domains
Antibiotics inhibition
Peptidoglycan binding

ABSTRACT

The penicillin-binding proteins are the enzyme catalysts of the critical transpeptidation crosslinking polymerization reaction of bacterial peptidoglycan synthesis and the molecular targets of the penicillin antibiotics. Here, we report a combined crystallographic, small-angle X-ray scattering (SAXS) in-solution structure, computational and biophysical analysis of PBP1 of *Staphylococcus aureus* (*sa*PBP1), providing mechanistic clues about its function and regulation during cell division. The structure reveals the pedestal domain, the transpeptidase domain, and most of the linker connecting to the "penicillin-binding protein and serine/threonine kinase associated" (PASTA) domains, but not its two PASTA domains, despite their presence in the construct. To address this absence, the structure of the PASTA domains was determined at 1.5 Å resolution. Extensive molecular-dynamics simulations interpret the PASTA domains of *sa*PBP1 as conformationally mobile and separated from the transpeptidase domain. This conclusion was confirmed by SAXS experiments on the full-length protein in solution. A series of crystallographic complexes with β-lactam antibiotics (as inhibitors) and penta-Gly (as a substrate mimetic) allowed the molecular characterization of both inhibition by antibiotics and binding for the donor and acceptor peptidoglycan strands. Mass-spectrometry experiments with synthetic peptidoglycan fragments revealed binding by PASTA domains in coordination with the remaining domains. The observed mobility of the PASTA domain in *sa*PBP1 could play a crucial role for *in vivo* interaction with its glycosyltransferase partner in the membrane or with other components of the divisome machinery, as well as for coordination of transpeptidation and polymerization processes in the bacterial divisome.

1. Introduction

Bacteria are resilient. Their ability to adapt to diverse ecological niches is due in large part to the robustness of their cell envelope. This envelope is a tightly integrated network of membranes, lipoproteins, and glycolipids organized around a structural peptidoglycan polymer [1,2]. In Gram-positive bacteria, such as the highly pathogenic *Staphylococcus aureus* [3], this polymer comprises its cell surface [4-6]. The importance to the bacterium of preserving the integrity of this peptidoglycan polymer is reflected by the structural diversity of antibiotic entities developed—including penicillin, fosfomycin, vancomycin, and polymyxin—that function by disrupting peptidoglycan biosynthesis [7]. The mechanism of the penicillins is irreversible acylation, by its β-lactam substructure, of the peptidoglycan crosslinking enzymes (historically, called penicillin-binding proteins, or PBPs) [8]. A major focus in the current study of PBP function is discernment of the precise molecular function of each PBP within the bacterial family [9]. *S. aureus* creates its complex and nearly spherical peptidoglycan with a spare ensemble of only four PBPs, of which two (*sa*PBP1 and

* Corresponding authors.
E-mail addresses: mobashery@nd.edu (S. Mobashery), xjuan@iqfr.csic.es (J.A. Hermoso).
[1] Present address: Instituto de Química, Universidad Nacional Autónoma de México, Ciudad Universitaria, 04510, Ciudad de Mexico.
[2] The first two authors contributed equally to this work.

https://doi.org/10.1016/j.csbj.2021.09.018

*sa*PBP2) are essential [10-12]. Addition of a fifth PBP (PBP2a) is a clinically significant antibiotic-resistance mechanism in methicillin-resistant *S. aureus* [13-16].

The growth and separation processes used by bacteria correlate with their cell shape. As a nearly spherical (coccus-shaped) bacterium, growth of the cell envelope of *S. aureus* is primarily the creation of a mid-cell septum, that ultimately fractures to release the parent and daughter cells as (transiently) hemisphere-shaped cells [16-18]. Peptidoglycan biosynthesis occurs by glycan-strand formation (tranglycosylase activity), followed by crosslinking (transpeptidase activity). Creation of the peptidoglycan of this septum is tasked to its two critical *S. aureus* PBPs, PBP1 (*sa*PBP1) and PBP2 (*sa*PBP2). These two PBPs function cooperatively within a multi-protein and multi-enzyme complex, termed the "divisome" [19,20]. Multiple divisome complexes organize against the inner membrane surface at mid-cell. A ring of new peptidoglycan is integrated into the existing peptidoglycan (a process facilitated by *sa*PBP3) at this circumference. A subsequent concentric and inwardly spiraling motion of multiple divisome complexes complete the septum [21]. *sa*PBP1 constructs the leading-edge septal peptidoglycan, possibly to create a substrate template for *sa*PBP2 [16,22]. The majority of the septal peptidoglycan mass arises through PBP2 catalysis.

Peptidoglycan is a polymer of glycan strands crosslinked through peptide stems and the peptide stems of the nascent peptidoglycan terminate with an -L-Lys(ε-Gly_5)-D-Ala-D-Ala sequence. Both *sa*PBP1 and *sa*PBP2 recognize the terminal -D-Ala-D-Ala motif, catalyze acyl-transfer of the penultimate D-Ala to the nucleophilic serine of their active site to form an acyl-enzyme (with the attendant release of the terminal D-Ala), and complete catalysis and crosslink formation by transfer of the D-Ala acyl moiety to a nucleophilic amine on an adjacent glycan strand. In *S. aureus* this amine is provided by the terminal glycine of the L-Lys(ε-$Gly)_5$ bridge peptide. *sa*PBP1 and *sa*PBP2 are differentiated in two key aspects. Firstly, *sa*PBP2 is a bifunctional class A PBP (aPBP), having both transglycosylase and transpeptidase active sites [23], while *sa*PBP1 is a monofunctional class B PBP (bPBP) having only transpeptidase activity. As a consequence, *sa*PBP1 must partner with a transglycosylase, a role played by the "shape, elongation, division and sporulation" (SEDS) protein FtsW. The substrate for *sa*PBP1 is the nascent glycan strand produced from Lipid II polymerization by FtsW [24]. There is a strong association of FtsW to *sa*PBP1 [25]. The FtsW:*sa*PBP1 complex functions as a key structural edifice of the divisome (Scheffers and Pinho, 2005). Fig. 1 shows this partnership. Second, *sa*PBP1 and *sa*PBP2 are distinguished by the presence of two PASTA domains in *sa*PBP1 (predicted from sequence analysis), while *sa*PBP2 does not contain those domains [26,27]. "PASTA" is an acronym for a "Penicillin-binding protein And Serine/Threonine kinase Associated" protein domain. PASTA domains are recognized as broadly encountered, as single or multiple repeats, among bacterial proteins [28,29]. Each PASTA domain comprises 65–70 amino acids organized as an N-terminal α-helix packed against a three-strands antiparallel β-sheet [30-34]. A key function of many PASTA domains is in protein–protein recognition [35], and as sensors of the cell-envelope status or stress by recognition of peptidoglycan structure [36,37]. We proposed recently that the PASTA domain of PBP2x of *Streptococcus pneumoniae* (*sp*PBP2x) could form an allosteric pocket that anchors nascent peptidoglycan and promotes catalysis [38]. Molecular-dynamic simulations of *sp*PBP2x demonstrated a stable intramolecular interaction between its PASTA domain repeat and its transpeptidase domain. The PASTA domain of the *S. pneumoniae* protein kinase StkP sequesters the proteins LytB and MapZ to facilitate cell constriction and separation [39]. PASTA domains in PBP2b from *Bacillus subtilis* strengthen its interaction with DivIB (in other organisms, FtsQ) protein to enable successful cell division [35].

The crystal structures of four of the PBPs of *S. aureus* (those of *sa*PBP2, PBP2a, *sa*PBP3, and *sa*PBP4) are solved [23,40-43]. Here, we report a structural, computational and biophysical analysis of the last remaining PBP of *S. aureus*, *sa*PBP1, with particular attention to the transpeptidation process and the intramolecular relationship of its PASTA domains to the other domains of this protein as an essential step toward dissecting the structure–function relationship of this fundamental PBP from *S. aureus*.

2. Materials and methods

2.1. Construction of pET24-PBP1 and purification of saPBP1

A soluble *S. aureus* PBP1 for overexpression in *E. coli* was designed using sequence alignment with *sp*PBP2x. Based on the sequence alignment, the first 64 amino acids and the 33 amino acids from the C-terminus were removed. The gene for this variant was amplified by PCR with primers ORB001 and ORB005 from *S. aureus* N315 genomic DNA and was ligated into the plasmid pET24a(+) using the restriction enzymes NdeI and XhoI (Primer sequences in Table S1). A stop codon was included at the 3′-end of the PCR product in order to express the enzyme without a His-tag. *E. coli* BL21 DE3 was transformed by the plasmid for overexpression of the protein. An overnight culture of *E. coli* BL21 DE3 (10 mL) inoculated 1 L of LB containing 30 μg mL^{-1} of kanamycin. The culture was grown at 37 °C with shaking (190 rpm) to an OD_{600} of 0.6 (approximately 3 h). Protein expression was induced (final concentration of 0.5 mM IPTG) by overnight culture at 16 °C. Cells were harvested by centrifuging at 6,000 *g* (15 min at 4 °C). The pellet was resuspended in 30 mL of Buffer A (25 mM HEPES, 150 mM NaCl pH 7.4) supplemented with 1 × Protease Inhibitor Cocktail (APExBio). The cells were disrupted with 10 cycles of sonification on ice (1-min pulse—40% duty cycle and output control 4—and 2-min rest with a Branson 450 Sonifier), followed by centrifugation at 18,000*g* (45 min at 4 °C). The supernatant was loaded onto a High S-Sepharose cation-exchange column (2.5 cm × 15 cm) equilibrated with Buffer A at 3 mL min^{-1}. Proteins were eluted with a linear gradient of 0.15–1.0 M NaCl using Buffer B (25 mM HEPES, 1 M NaCl pH 7.4) at 1.5 mL min^{-1} (total volume of 0.3 L). The fractions containing the *sa*PBP1 (as determined by SDS-PAGE) were combined and concentrated to a final volume of 3 mL using a 10 kDa-cutoff centrifugal filter. The concentrate was loaded onto a Sephacryl S200 size-exclusion column (1.5 cm × 90 cm). Proteins were eluted at 0.4 mL min^{-1} with 160 mL Buffer A. The fractions containing pure PBP1 were combined and concentrated using a 10 kDa-cutoff centrifugal filter.

2.2. Construction of pET41ST-$PASTA_{PBP1}$ and purification of $PASTA_{PBP1}$

The commercial vector pET41b(+) was modified by putting a Strep-tag and a tobacco etch virus (TEV) protease cleavage site at the downstream of the enterokinase cleavage site to make the recombinant proteins susceptible to processing by the TEV protease. Double-stranded DNA fragments synthesized with a set of oligomers (CK171/CK172) were ligated with NcoI/XhoI-digested pET41b(+). The resulting vector was named pET41ST. The DNA fragment encoding the PASTA domain (Ala597 to Ser713) of *S. aureus* PBP1 was cloned following a restriction-enzyme-independent method (the fast-cloning approach). Two sets of primers containing overlapped sequences (~17 nucleotides) were used to amplify the vector pET41ST (primers CK2645 and CK266) and the PASTA domain (primers CK173 and CK174) from pET24-PBP1 described above (Primer sequences in Table S1). DpnI

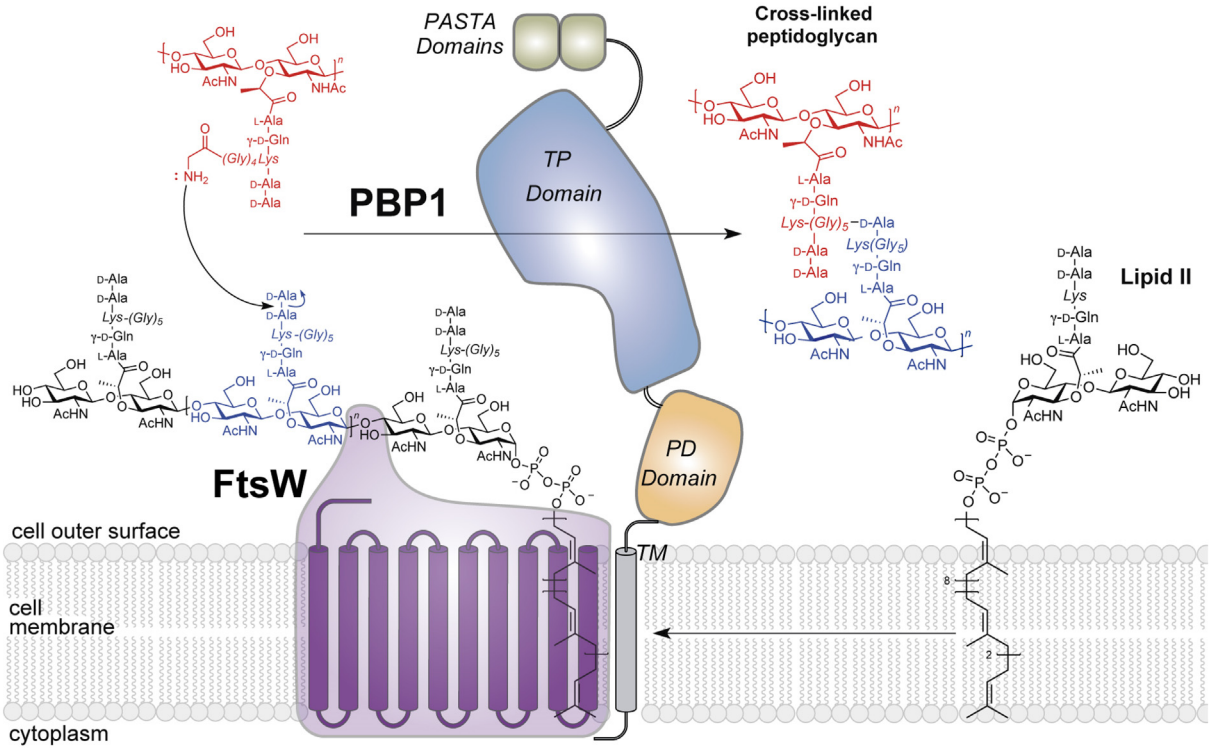

Fig. 1. Schematic representation of *sa*FtsW:*sa*PBP1 complex. The FtsW:PBP1 complex is involved in polymerization of Lipid II and crosslinking of the nascent peptidoglycan into the growing edge of the cell wall. Polymerization is performed by the SEDS protein FtsW. The transpeptidase reaction of *sa*PBP1 involves acyl-enzyme formation at S314 from the terminal -D-Ala-D-Ala motif of the peptide stem.

(1 μL) was added to each PCR product, and two PCR products were mixed at 1:1 or 1:2 ratios (vector:insert), followed by incubation for 1 h at 37 °C to degrade the template DNAs. *E. coli* DH5α was transformed with each mixture. The two DNA fragments in the mixture would be ligated spontaneously in the cell. The resulting plasmid pET41ST- $PASTA_{PBP1}$ was confirmed by DNA sequencing covering from the T7 promoter to the stop codon of the gene. The plasmid was inserted into BL21Star (DE3) to overexpress $PASTA_{PBP1}$ with a 6 × His-tag, a GST-tag, a Strep-tag and a TEV cleavage site at the N-terminus. The protein was produced by induction with 0.4 mM IPTG at OD_{600} of 0.6 and incubation for 4 h at 30 °C.

Cells were harvested and disrupted in lysis buffer (50 mM Tris-HCl, 50 mM NaCl pH 7.5, with 5% glycerol, 10 mM $MgSO_4$, 2 mM ATP, 1 mM DTT, 50 μg mL^{-1} lysozyme, 50 μg mL^{-1} DNase I, 1 × protease inhibitor cocktail), as described above. The supernatant was applied to a Glutathione Sepharose™ 4 Fast Flow column (Cytiva) equilibrated with washing buffer I (50 mM Tris-HCl, 100 mM NaCl pH 7.5), to purify the recombinant protein via the GST-tag, following the manufacturer's instruction. The fractions containing His-GST-Strep-tagged $PASTA_{PBP1}$ were pooled and concentrated to a total volume of 5 mL. The protein was run through a Ni-NTA resin (Protino) with stepwise elution of 20 mM, 200 mM, 500 mM and 800 mM imidazole in 50 mM Tris-Cl, 150 mM NaCl pH 8.0 buffer. The fractions eluting at 500 mM and 800 mM imidazole were combined. Repeated filtration with an Amicon Ultra 10 kDa-cutoff filter removed imidazole. The concentrated protein (3 mg mL^{-1}) was incubated with His-tagged TEV protease (purchased from MCLAB) as a 1:100 TEV protease:target protein ratio at 4 °C for 24 h to remove all tags. The $PASTA_{PBP1}$ protein was separated from the tags, His-tagged TEV protease, and non-cleaved tagged-$PASTA_{PBP1}$ using a Ni-NTA column. The flow-through fraction and the 20 mM imidazole-washing fraction were collected. The $PASTA_{PBP1}$ purity was determined with SDS-PAGE and its yield was determined by BCA assay.

2.3. Synthetic compounds

Synthetic peptidoglycans **1**–**3** were prepared for this study by multi-step syntheses reported previously [44-46].

2.4. Non-denaturing mass spectrometry

Prior to non-denaturing mass spectrometry, the active site of 10 μM *sa*PBP1 was covalently labelled by incubating the protein with 300 μM penicillin G (penG) for 10 min at room temperature. The penG-labelled PBP1 (PBP1-penG) was separated from unbound PenG with Zeba Desalting Column (Thermo Fisher Scientific). $PASTA_{PBP1}$, PBP1 and PBP1-penG were buffer-exchanged to 1 M ammonium acetate, pH 6.6, with Zeba Desalting Columns. Mass spectrometry was performed as described [47,48]. Prior to injection of the samples into the mass spectrometer, the proteins were preincubated as follows: 1 μM of $PASTA_{PBP1}$ with 50 μM of the compounds for 1 h at room temperature and 10 μM of PBP1 with 200 μM of the compounds for 2 h at room temperature.

2.5. Crystallization of saPBP1

Crystallization screenings were performed using high-throughput crystallization techniques in a NanoDrop robot using Innovadyne SD-2-microplates (Innovadyne Technologies, Inc.) and screening using JBScreen $PACT^{++}$, JBScreen Classic 1 to 4, JBScreen $JCSG^{++}$ 1 to 4 (Jena Bioscience), Crystal Screen, Crystal Screen 2, SaltRx HT, Index HT (Hampton Research), and Wizard Cryo (Rigaku) protocols. The conditions that produced crystals were optimized by sitting-drop vapor diffusion method at 290 K by mixing 1 μL of protein solution and 1 μL of precipitant solution,

equilibrated against 150 μL of precipitant solution in the reservoir chamber. Crystals of PBP1 were obtained in 2.1 M DL-malic acid pH 7.0 at a concentration of 10 mg mL^{-1}. Crystals of PBP1·penicillin G complex were obtained by co-crystallization in 1.6 M sodium citrate at a concentration of 11 mg mL^{-1}. The complex with piperacillin was obtained by soaking the PBP1 crystals in the crystallization solution containing 2 mM of piperacillin for 30 min. The complex with pentaglycine was obtained by soaking the PBP1 crystals overnight in the crystal solution containing 0.45 mM of pentaglycine.

2.6. Crystallization of $PASTA_{PBP1}$

Crystallization screenings were performed using high-throughput crystallization techniques in a NanoDrop robot with Innovadyne SD-2-microplates (Innovadyne Technologies, Inc.). Crystals of PBP1-PASTA domain (amino acids 597–713) were obtained in different crystallization conditions by the sitting-drop method at 291 K at 7.2 mg mL^{-1} of protein. The best crystals were obtained in a precipitant solution consisting of 30% (v/v) PEG 400, 0.1 M HEPES free acid/Sodium hydroxide pH 7.5, 5% (w/v) PEG 3000, and 10% glycerol.

2.7. Data collection, structure solution, model building and refinement of saPBP1

Diffraction data were collected in the XALOC beamline at the ALBA synchrotron (Barcelona, Spain) using a Pilatus 6 M. The data sets were processed with XDS and Aimless [49,50]. PBP1 diffraction patterns presented anisotropy that was corrected by using the STARANISO server [51] (http://staraniso.globalphasing.org/cgi-bin/staraniso.cgi) with a surface threshold of 0.6 $_{w}CC_{1/2}$ and/or the Local mean I/σ(I) of 1.2, implemented through the autoProc pipeline [52]. The structures were solved by the molecular-replacement method with Molrep [53], using the *sa*PBP1 structure (PDB code 5TRO) as template. The coordinates were refined using Phenix [54]; Refmac from CCP4 [55]; and modelled using Coot [56]. Data refinements are given in Table1.

2.8. Data collection, structure solution, model building and refinement of $PASTA_{PBP1}$

X-ray data sets were collected from frozen crystals at 100 K with PILATUS detector at beamline XALOC (ALBA Synchrotron, Barcelona, Spain). Data processing and scaling used XDS [49] and Aimless from the CCP4 program suite [57]. The structure was solved by molecular replacement as implemented by the program Phaser [58]. The search model was based on the two PASTA domains from PBP2x of *S. pneumoniae* (PDB code 5OAU). The model was subjected to iterative cycles of model building and refinement with Coot and Phenix, respectively. Statistics for the crystallographic data and the structure solution are in Table1.

2.9. MALDI-TOF experiment

*sa*PBP1 crystals were washed repeatedly with the crystallization solution and then dissolved in water. Samples were diluted at a 1:1 ratio (v/v) with matrix solution (50% saturated sinapinic acid in 70% (v/v) aqueous acetonitrile and 0.1% trifluoroacetic acid). A 1.0 μL aliquot of this mixture was manually deposited onto a 386-well OptiTOF™ Plate (ABSciex, Foster City, CA) and allowed to dry at room temperature. The spectrum was acquired on an Abi 4800 MALDI TOF/TOF mass spectrometer (SCIEX, Foster City, CA) in positive ion linear mode (ion acceleration voltage of 25 kV) using AB Sciex 4000 Series Data Explorer control and processing software. The detection mass range was *m*/*z* 20,000–150,000.

2.10. Protein-protein docking

The protein–protein docking was computed with the ZDOCK program implemented on the online server [59,60].

2.10.1. Protein modeling and molecular-dynamics simulations

The three-dimensional coordinates of the missing stretch of the loop spanning residues 582–633 were modeled computationally based on secondary-structure prediction with the program Maestro (https://www.schrodinger.com/products/maestro). The X-ray structure of the transpeptidase (TP) and PASTA domains were linked to each other with the modeled sequence. This full-length model was immersed in a rectangular box of TIP3P water molecules, energy-minimized, and subjected to MD simulation using PMEMD module of Amber18 [61], following a reported protocol [42]. Amber ff14SB provided forcefield parameters. Various conformations of the loops were generated with the program Prime (Schrödinger Suite 2019–4) using the *sp*PBP2x crystal structure as template.

2.10.2. Model of FtzW-PBP1-Peptidoglycan ternary complex in S. aureus

The model used the coordinates of the *T. thermophiles* PBP2·RodA complex (PDB code: 6PL6) [62]. The final snapshot from the 1-μs MD trajectory of *sa*PBP1 (this study) was extracted and superimposed on the *tt*PBP2. The single predicted transmembrane helix of *sa*PBP1 was modeled using *tt*PBP2 helix as template. FtzW was modeled using RodA as template (23% identity and 41% similarity). The membrane model (POPC: 1-palmitoyl-2-oleoyl-*sn*-glycero-3-phosphocholine) was constructed with the Desmond System Builder program (Version 6.1, D. E. Shaw Research, NY). The conformation of the cross-linked peptidoglycan from the previous study [42] was modeled to the active site of *sa*PBP1 after superimposition of the active site of *sa*PBP2a-peptidoglycan complex to the *sa*PBP1.

2.10.3. Small-Angle X-ray Scattering (SAXS) data collection, processing and modelling of full-length saPBP1

Experiments were performed at the beamline B21 of the Diamond Light Source (Didcot, UK) [63]. A sample of 40 μL of PBP1 at concentration of 4 mg/ml were delivered at 20 °C via an in-line Agilent 1200 HPLC system in a Superdex 200 Increase 3.2 column, using 25 mM HEPES pH 7.4 and 150 mM NaCl as the running buffer. The continuously eluting samples were exposed for 300 s in 10 s acquisition blocks using an X-ray wavelength of 1 Å, and a sample to detector (Eiger 4 M) distance of 3.7 m. The data covered a momentum transfer range of $0.0032 < q < 0.34$ Å-1. The frames recorded immediately before elution of the sample were subtracted from the protein-scattering profiles. The Scåtter software package (www.bioisis.net) was used to analyse data, buffer-subtraction, scaling, merging and checking possible radiation damage of the samples. The Rg value was calculated with the Guinier approximation, assuming that at very small angles $q < 1.3/Rg$. The particle distance distribution, Dmax, was calculated from the scattering pattern with GNOM, and shape estimation was carried out with DAMMIF/DAMMIN, all these programs are included in the ATSAS package [64]. The proteins molecular mass was estimated with GNOM. Interactively generated PDB-based homology models were made using the program COOT from the CCP4 Program suit [57] using as templates the crystal structures of the proteins obtained from this work, and placed into the SAXS envelope. The real-space scattering profile of the homology model

Table 1
X-ray Data collection and refinement statistics.

	PBP1	PBP1:piperacillin complex	PBP1:penicillin G complex	PBP1:pentaglycine complex	PBP1-PASTA
Data collection statistics					
Wavelength (Å)	0.97926	0.97925	0.97918	0.97926	0.97918
Space group	P 2_1 2_1 2	P 6_4 2 2	P 6_4 2 2	P 2_1 2_1 2	P 2_1 2_1 2_1
Unit cell dimensions					
a, *b*, *c* (Å)	311.86, 197.15, 221.6	178.69, 178.69, 223.65	180.65, 180.65, 223.47	313.99, 198.19, 220.90	39.97, 80.56, 90.42
α, β, γ (°)	90,90,90		90,90,120	90,90,90	90,90,90
Resolution range (Å)	49.00–3.32 (3.33–3.32)	47.40–3.24 (3.25–3.24)	47.51–2.74 (2.75–2.74)	49.32–3.94 (3.96–3.94)	45.21–1.51 (1.54–1.51)
No. of unique reflections	185,164 (1,852)	34,090 (336)	57,176 (570)	121,463 (1,211)	46,753 (2,309)
Completeness (%)	92.0 (93.3)	99.9 (100)	100 (100)	99.8 (99.5)	100.0 (100.0)
Multiplicity	8.4 (6.5)	29.7 (16.3)	24.5 (22.3)	13.0 (13.6)	13.0 (13.3)
CC1/2	0.996 (0.331)	0.997 (0.313)	0.999 (0.361)	0.964 (0.313)	1.000 (0.948)
R_{pim}	0.074 (1.083)	0.072 (2.314)	0.039 (1.756)	0.332 (2.380)	0.012 (0.193)
Avg. I/σ (I)	9.9 (0.8)	11.6 (0.4)	17.8 (0.4)	5.7 (1.0)	30.8 (4.0)
Data with anisotropic correction (STARANISO server)					
Anisotropic resolution (Å) (direction)	3.598 (a*)	3.843 (0.894 a* – 0.447b*)	3.170 (0.894 a* – 0.447b*)	5.448 (a*)	–
	4.269 (b*)	3.843 (b*)	3.170 (b*)	4.663 (b*)	
	3.005 (c*)	2.863 (c*)	2.507 (c*)	3.110 (c*)	
Resolution after correction	49.01–3.03 (3.42–3.03)	47.40–3.03 (3.31–3.03)	47.51–2.59 (2.85–2.59)	49.32–3.36 (3.76–3.36)	–
No of unique reflection (ellipsoidal)	145,321 (7266)	26,360 (1318)	45,182 (2,260)	86,448 (4,322)	–
Completeness ellipsoidal (%)	89.9 (73.1)	95. 1 (81.4)	96.3 (83.2)	89.1 (64.6)	–
Completeness spherical (%)	55.3 (9.3)	63.4 (13.9)	67.5 (14.1)	74.2 (17.4)	–
Multiplicity	8.9 (9.8)	32.1 (39.5)	24.7 (27.3)	44.0 (7.8)	–
Avg. I/σ (I)	11.0 (2.2)	14.3 (1.8)	22.1 (2.0)	7.5 (1.9)	–
R_{pim}	0.058 (0.401)	0.058 (0.468)	0.030 (0.420)	0.195 (0.785)	–
CC1/2	0.997 (0.735)	0.998 (0.744)	0.999 (0.706)	0.982 (0.408)	–
Refinement Statistics					
Resolution range (Å)	48.89–3.03	46.84–3.03	47.26–2.59	49.27–3.37	40.28–1.51
R_{work}/R_{free}	0.211/0.246	0.211/0.278	0.205/0.241	0.199/0.245	0.167/0.197
No. of atoms					
Protein	48,489	7756	7697	47,732	1873
Water	50	–	39	6	166
Ligand	168	84	152	179	1
RMS deviations					
Bond length (Å)	0.014	0.013	0.014	0.014	0.014
Bond angles (°)	1.92	1.91	1.91	1.68	1.74
Ramachandran plot					
Favored/outlier (%)	87.17/1.21	88.45/0.82	90.98/0.52	90.92/1.05	99.13/0.00
Monomers per AU	12	2	2	12	2
PDB code	7O49	7O4A	7O4B	7OK9	7O4C

[a]Statistics are for data that were truncated by STARANISO to remove poorly measured reflections affected by anisotropy.
Numbers in parentheses correspond to the outer resolution shell.

was computed with the program FoXS [65]. The overall parameters and the SAXS modelling results are summarized in Table 2.

3. Results

3.1. Three-dimensional structure of PBP1 from S. aureus

*sa*PBP1 is a multi-domain protein containing 744 amino-acid protein and shows a total of four segments and four domains. This total includes a predicted short N-terminal cytosolic segment (residues 1–11), a transmembrane segment (amino acids 12–38), the pedestal domain (PD, amino acids 39–244), the transpeptidase domain (TP, amino acids 245–585), a linker segment (amino acids 586–596) connecting the two PASTA domains (amino acids 597–713), and a C-terminal tail segment (amino acids 714–744) (Fig. 2A). The gene for the *sa*PBP1 protein construct spanning amino acids 65–713 (excising the cytoplasmic and transmembrane segments and the C-terminal disordered tail located after the PASTA domains) was cloned, expressed, and purified (Figure S1). Crystals of the protein (10 mg mL^{-1}) were obtained from 2.1 M DL-malic acid pH 7.0 and diffracted to 3.0-Å resolution. The three-dimensional structure of *sa*PBP1 was solved by molecular replacement using a partial previous model (that of the pedestal and TP domains of *sa*PBP1; PDB code 5TRO) provided by the Center for Structural Genomics of Infectious Diseases (see Methods and Table1). Our crystals presented a large unit cell with 12 independent molecules in its asymmetric unit. The 12 protein monomers in the asymmetric unit have similar structures (root-mean-square deviation (RMSD) values of 0.08–0.11 Å for Cα atom superimposition (Figure S2). The overlap of the previous partial structure for *sa*PBP1 with our structure shows good similarity (rmsd of 0.32 Å for 380 Cα atoms superimposition).

The electron-density maps from our *sa*PBP1 crystals allowed us to unambiguously build a final model containing the pedestal domain, the transpeptidase domain, and most of the linker connecting the PASTA domains, but not the PASTA domains themselves (Fig. 2B). MALDI-TOF experiments using dissolved *sa*PBP1 crystals indicated that they contained the full construct (Figure S3), confirming that the PASTA domains were present (not proteolyzed during handling) and therefore, PASTA domains in the crystallized protein were either mobile or disordered. The pedestal domain of

Table 2
SAXS Data Collection and derived parameters.

Data collection parameters	
Instrument	Diamond Light Source beamline B21 (Harwell Campus, UK)
Wavelength (Å)	1
q-range ($Å^{-1}$)	0.0032–0.38
Exposure time (s)	300
Concentration (mg ml^{-1})	4
Temperature (K)	293
Structural parameters	
Protein	PBP1
Rg (Å) (from Guinier)	34.88 ± 0.03
Rg (Å) (from P(r))	34.90 ± 0.03
Dmax (Å)	128 ± 0.2
Molecular mass determination	
MM (kDa) from Porod volume	74
Calculated MM (kDa) from sequence	72.12
Software employed	
Data processing	Scåtter/PRIMUS/ GNOM
Ab initio analysis / Averaging	DAMMIF, DAMMIN/DAMAVER
Computation of model intensities	FoXS
3D graphics representations	PyMOL

*sa*PBP1 is formed by two subdomains—the anchor and the head—as observed in other bPBPs (Fig. 2B) [62]. The main differences with respect to Cα atom superimposition are in the pedestal domain, where variations are observed in the disposition of the head subdomain and in the loop 209–237 (L209–237) from the anchor subdomain. While in all our cases this loop is oriented towards the TP domain, two distinct conformations are observed among the independent monomers. In one monomer set the backbone of the loop runs in an anti-parallel manner (chains A, C, G, H, I, and J, Figure S2) while in the other monomer set the loop backbone is crossed (chains B, D, E, F, K, and L).

The closest structural homologues of *sa*PBP1 are the PBP2x proteins from *S. pneumoniae* (*sp*PBP2x; PDB code 5OAU; rmsd of 1.359 Å for 353 Cα superimpositions) and from *Streptococcus thermophilus* (*st*PBP2x; PDB code 5U47; rmsd of 0.70 Å for 461 Cα superimpositions). Comparison of *sa*PBP1 with *sp*PBP2x (Figs. S4 and S5) indicated differences in both the PD and the TP domains (Fig. 2C, D and S4), notwithstanding a 95% sequence identity for the shorter stretches. The most relevant difference in the pedestal domain is the profoundly different conformation and disposition of Loop 209–237 (L209–237). In both *sp*PBP2x (residues 229–258) and *st*PBP2x (residues 234–263) this loop has an extended conformation. In contrast, the loop conformation in *sa*PBP1 shows an angular rotation of >140° and folds onto the TP domain (Fig. 2C). The tip of the L209–237 loop in *sa*PBP1 (amino acids 215–225) occupies the position observed for the linker and the first PASTA domain (P1) in the crystal structures of *sp*PBP2x and *st*PBP2x (Fig. 2C and S4). In this conformation the L209–237 loop does not preserve the interactions with the TP domain that were observed for the PASTA domains with TP domain in *sp*PBP2X (Figure S6). Differences are also observed between the active sites of *sa*PBP1 and *sp*PBP2x (Fig. 2D). The different structural elements in *sa*PBP1 (the α12 helical turn η6, and the conformation of the

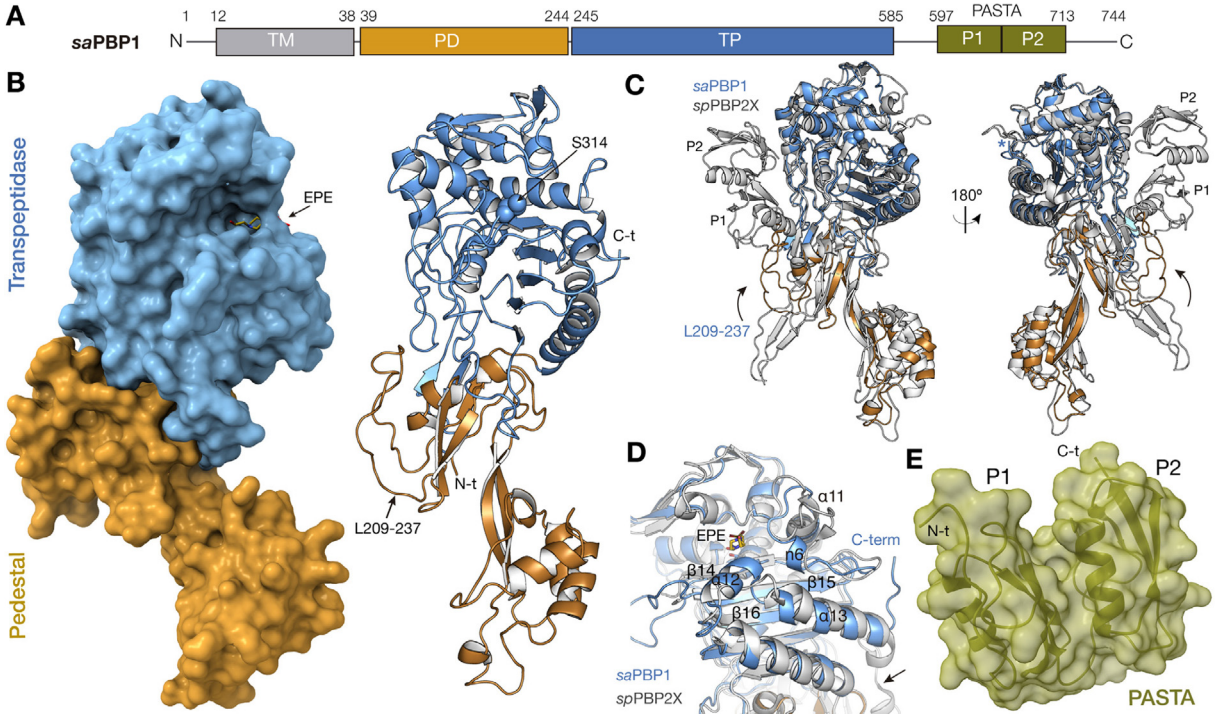

Fig. 2. Three-dimensional structure of *sa*PBP1. (A) The *sa*PBP1 modular organization. (B) Molecular surface and ribbon representation of the crystal structure of *sa*PBP1 with domains colored according to panel A. The HEPES buffer molecule (EPE), bound close to the active site, is shown in capped sticks colored by atom types (carbons in yellow). The catalytic S314 is labeled and is depicted as blue spheres. The position for Loop 209–237 is indicated by an arrow (at 7o'clock). (C) Structural superimposition of *sa*PBP1 (colored as in panel B) and *sp*PBP2x (colored uniformly in gray) highlights similarities and differences. The two extremes of the spatial dispositions of L209–237 (saPBP1 numbering) are highlighted by the curved arrow. The position of the C-terminal linker in *sa*PBP1 is indicated by a blue asterisk (at 10o'clock of the right image). PASTA domains of *sp*PBP2X are labeled P1 and P2. (D) Differences in the active sites of *sa*PBP1 (blue) and *sp*PBP2x (gray) are depicted. The EPE molecule is displayed as yellow sticks. A different orientation of the linker connecting the TP domain with PASTA domains in *sa*PBP1 (C-term labeled) versus *sp*PBP2x (highlighted with an arrow) is observed. (E) Three-dimensional structure of the PASTA domains of *sa*PBP1. (For interpretation of the references to color in this figure legend, the reader is referred to the web version of this article.)

loop connecting α11 with β14) (Figure S5) give a narrower active-site cavity compared to the cavity of *sp*PBP2x. This difference is especially relevant to the acceptor-strand site (Figures S7A and S7B). The linker connecting the TP and the PASTA domains in *sa*PBP1 is disposed differently compared to *sp*PBP2x (Fig. 2D).

3.2. High-resolution crystal structure of PASTA domains of saPBP1

The absence of structural information about the two PASTA domains prompted further effort. Thus, we cloned DNA for expression of the two *sa*PBP1 PASTA domains by themselves (corresponding to amino acids 597–713). The gene was expressed and the protein was purified to homogeneity (Figure S1). High-throughput crystallization assays gave a single crystallization hit. After several rounds of optimization, crystals diffracting at 1.5-Å resolution were obtained (Table 1). The two PASTA domains (P1, amino acids 597–655 and P2, amino acids 656–713) showed the precedented PASTA folding of one α-helix facing a three-stranded β-sheet (Fig. 2E). P1 and P2 interact with each other through polar interactions (notably, a salt-bridge between K649 and D670) and through a core of hydrophobic residues linking the exposed side of the β-sheet from P1 with the α-helix from P2 (Figure S8A). Comparison of these PASTA domains with that of *sp*PBP2x reveals small differences in the disposition of the regions connecting the secondary-structure elements (rmsd of 1.68 Å for 98 Cα atoms: Figure S8B). The hydrophobic core that links P1 and P2 is conserved in *sp*PBP2x (Figure S8B). However, comparison to the PASTA domains of *S. aureus* Ser/Thr kinase PrkC (PDB code 3PY9) shows that the hydrophobic residues that glue the two PASTA domains in *sa*PBP1 are replaced by charged residues in the three PASTA domains of *sa*PrkC. These substitutions preclude formation of the compact fold observed in *sa*PBP1 and accounts for the extended and labile conformation seen for the PASTA domains of *sa*PrkC (Figure S8C).

3.3. Computational modeling of the saPBP1 construct

The unification of the two crystallographic structures was done by computational analyses. The tandem PASTA domains of *sp*PBP2x show close interaction with its TP domain. The crevice found at the interface of these domains in *sp*PBP2x is an allosteric site (confirmed by kinetic studies) that binds an intact β-lactam antibiotic as a surrogate for the terminal section of the peptide stem (seen by X-ray crystallography) [66,67]. X-ray-guided computational modeling suggested the D-Ala terminus of the full-length stem peptide of the nascent peptidoglycan as the endogenous ligand for this site [38]. We investigated computationally whether the free-standing PASTA domain repeats of *sa*PBP1 could occupy the TP domain surface as was seen for the *sp*PBP2x. The X-ray structure for the tandem repeat of the *sa*PASTA (amino acids 597–713) was evaluated as a "ligand" for binding to the apo *sa*PBP1 surface using the protein–protein docking program ZDOCK [59,60]. The extensive protein–protein surface complementarity between TP and PASTA domains of *sp*PBP2x was the control for this docking analysis. Indeed, the docking analysis reproduced the TP-PASTA interaction of *sp*PBP2x seen in the X-ray structure (not shown). In contrast, none of the top-scoring poses for docking the *sa*PASTA to *sa*PBP1 simulated the PASTA·TP interaction of *sp*PBP2x. Thus, we examined a complementary computational approach. A *sa*PBP1 model was generated by linking the TP domain of *sa*PBP1 and that of the PASTA-domain repeat and the linker residues (13 amino acids; Leu586–Glu598) to simulate the X-ray structure conformation of *sp*PBP2x (Movie S1). Although manual placement of the PASTA domains onto the TP domain in *sa*PBP1 achieved a conformation similar to that of *sp*PBP2x, the model did not reproduce the fit between the TP and PASTA domains of *sp*PBP2x. This failure was the consequence of steric hindrance of L209–237 as observed in the *sa*PBP1 crystal (Fig. 2). We generated 10 different conformational models. Each of the 10 protein models was immersed in a rectangular box of water, energy-minimized, and simulated for 20 ns. Each simulation showed displacement of the PASTA domains from its initial position, further arguing that close contact of the *sa*PASTA with the TP domain is not a stable interaction (Movie S2). We also investigated whether an extended conformation of L209–237 could favor this interaction by simulating the dynamics of 10 models of *sa*PBP1 with the extended conformation of Loop 209–237 (based on *sp*PBP2x: Fig. 2C) (protocol as described above). Once again, a stable interaction of the PASTA domains with the TP domain was not seen (Movie S3). Then, one of these starting conformations was evaluated using a 1 μs accelerated MD analysis [68]. The overall conformational landscape showed the PASTA domains keeping their compact fold, but exploring a variety of poses adjacent to the TP domain (Movie S4). Consequently, computational analyses agree with the crystallographic results, indicating a radically different positioning of PASTA domains in *sa*PBP1 compared with that observed for *sp*PBP2x.

3.4. SAXS studies on saPBP1 in solution

SAXS (Small Angle X-ray Scattering) data were collected and analyzed for *sa*PBP1 in solution (Table 2) to obtain low-resolution shape conformation. The protein behaved well during the SAXS measurement, and the Guinier regions were linear, in line with a monodisperse monomeric sample. The SAXS scattering curve and distance distribution are depicted in Fig. 3A and 3B. The result revealed the organization of *sa*PBP1 protein in solution, providing information on disposition of PD, TP and PASTA domains. The envelope clearly shows how the TP domain acts as a central core from which protrudes the PD and PASTA domains (Fig. 3C). To ease the visualization of the protein distribution inside the SAXS envelope, a full-length model of soluble *sa*PBP1 was created based on our crystallographic structures (see section before) and fitted into the SAXS envelope. The main modification from the computational model was displacing the position of the loop that joins the PASTA domains to the TP domain, to match the SAXS envelope. The PASTA domains in the model are ~25 Å from the TP domain in a disposition dramatically distinct from that observed for *sp*PBP2x (Fig. 3D). Interestingly, the compact structure of the PASTA domains observed by X-ray crystallography is preserved in solution. Even the crevice formed at the interface between P1 and P2 domains was clearly seen in SAXS envelope (Fig. 3C). It is noteworthy that superimposition of SAXS model onto the 12 independent molecules of our *sa*PBP1 crystal places the PASTA domains along the large cavities observed in the crystal packing, but with some clashes among the PASTA domains from different molecules. This fact could explain the lack of structural information for the PASTA domains in the *sa*PBP1 crystal structure.

In summary, crystallographic, computational and solution studies strongly support a distinct arrangement for the PASTA domains in *sa*PBP1 compared with previous examples observed in PBP2x (from *S. pneumoniae* or *S. thermophilus*). In *sa*PBP1 the PASTA domains would not be located close to the TP, but separated, thanks to the flexible linker connecting both regions.

3.5. Peptidoglycan binding to saPBP1

The PASTA domains of the bacterial protein kinases of *Bacillus subtilis* and *S. pneumoniae* bind weakly peptidoglycan fragments [69,70]. While the very different composition of the kinase PASTA domains compared to the PBP PASTA domains suggests different functions for the two types of PASTA domains, we assessed the

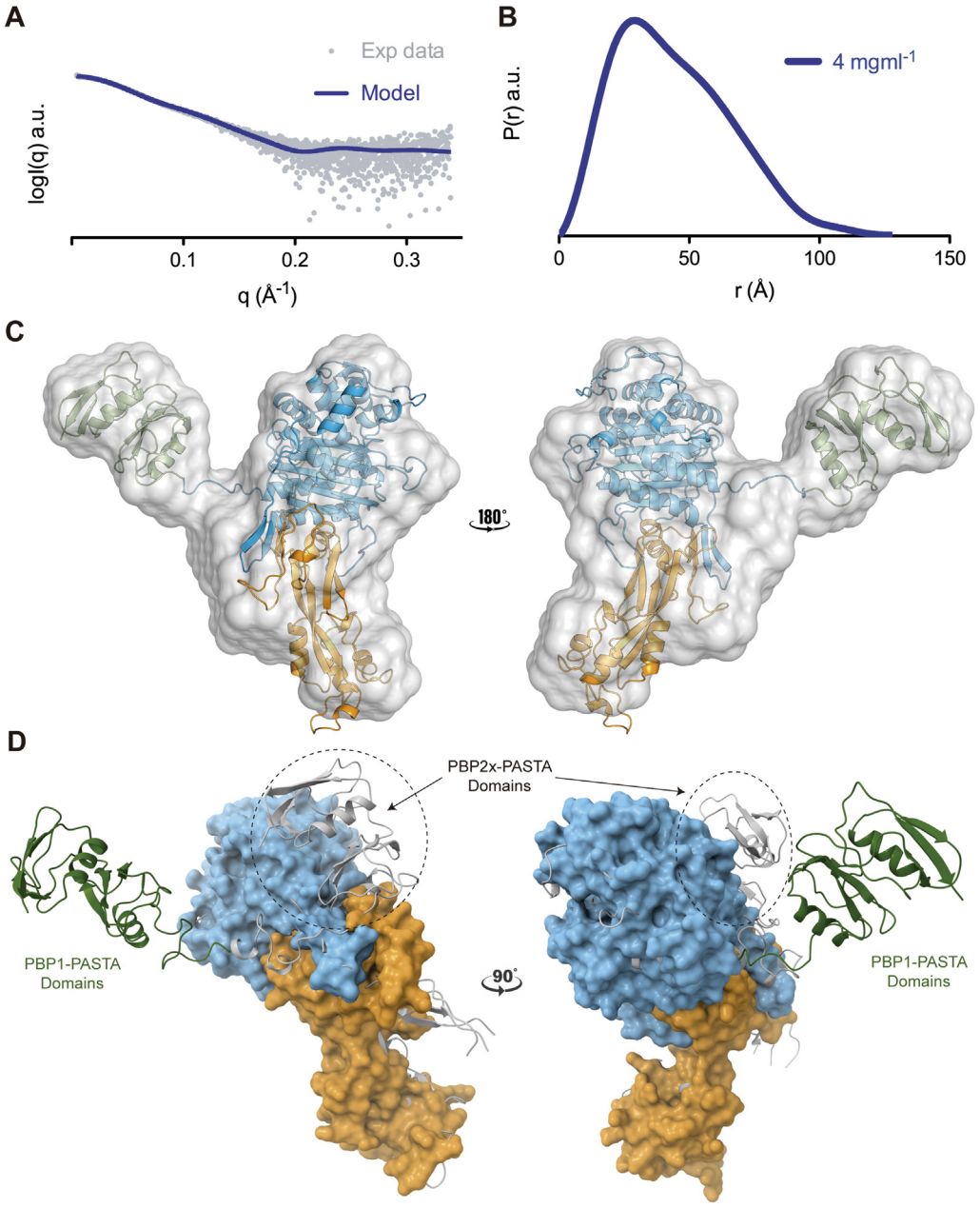

Fig. 3. Analysis by SAXS of *sa*PBP1 in solution. (A) Fit of the experimental scattering curve (gray dots) and theoretical scattering (blue line) computed for the model of *sa*PBP1 at 4 mgml^{-1}. (B) Plot showing the normalized pair-distance distribution function P(r) for *sa*PBP1 (blue graph) reflecting the distance distribution. (C) Superimposition on the *ab initio*-determined SAXS envelope (pale gray) for *sa*PBP1 with its crystal structure-based model (domains colored as in Fig. 2). (D) Structural comparison of the *sa*PBP1 composite model onto the *sp*PBP2x crystal structure (PDB code 5OAU), where *sa*PBP1 is represented by its molecular surface for TP and PD domains and by ribbon for the linker and PASTA domains (colors as in panel C). *sp*PBP2x is represented a gray ribbon. (For interpretation of the references to color in this figure legend, the reader is referred to the web version of this article.)

ability of the synthetic peptidoglycan fragments **1**, **2**, and **3** (Fig. 4A) to bind to *sa*PBP1. Since peptidoglycan binding may occur to the PASTA domains and/or the active site, a series of experiments was required. Native mass-spectrometry experiments were set up using the purified PASTA domains and soluble *sa*PBP1 with its active site modified by penicillin G (so as to exclude peptidoglycan binding at the active site). The experimental masses of the tandem PASTA domains, *sa*PBP1, and *sa*PBP1 modified by penicillin G were 12,687 Da (calcd 12,687 Da), 72,254 Da (calcd 72,255 Da), and 72,589 Da (calcd 72,590 Da), respectively (Fig. 4). Weak binding (3–4%) of the synthetic peptidoglycans **1**–**3** occurred to the PASTA domains (Fig. 4B–E). Acylation of the active site of PBP1 by penicillin G was stoichiometric (Fig. 4F and G). Binding of the peptidoglycan fragments to *sa*PBP1 modified by penicillin G was higher than to PASTA domains by themselves (5–12%: Fig. 4G–J). The natural nascent peptidoglycan, in contrast to the minimalist synthetic samples, is a polymeric entity. That observed binding is significant, notwithstanding the weak nature of binding to the synthetic peptidoglycan. The binding of the polymeric peptidoglycan with the surface of PBP1 is undoubtedly multivalent. The data provided herein argue that the multivalent binding involves the PASTA and the TP domains.

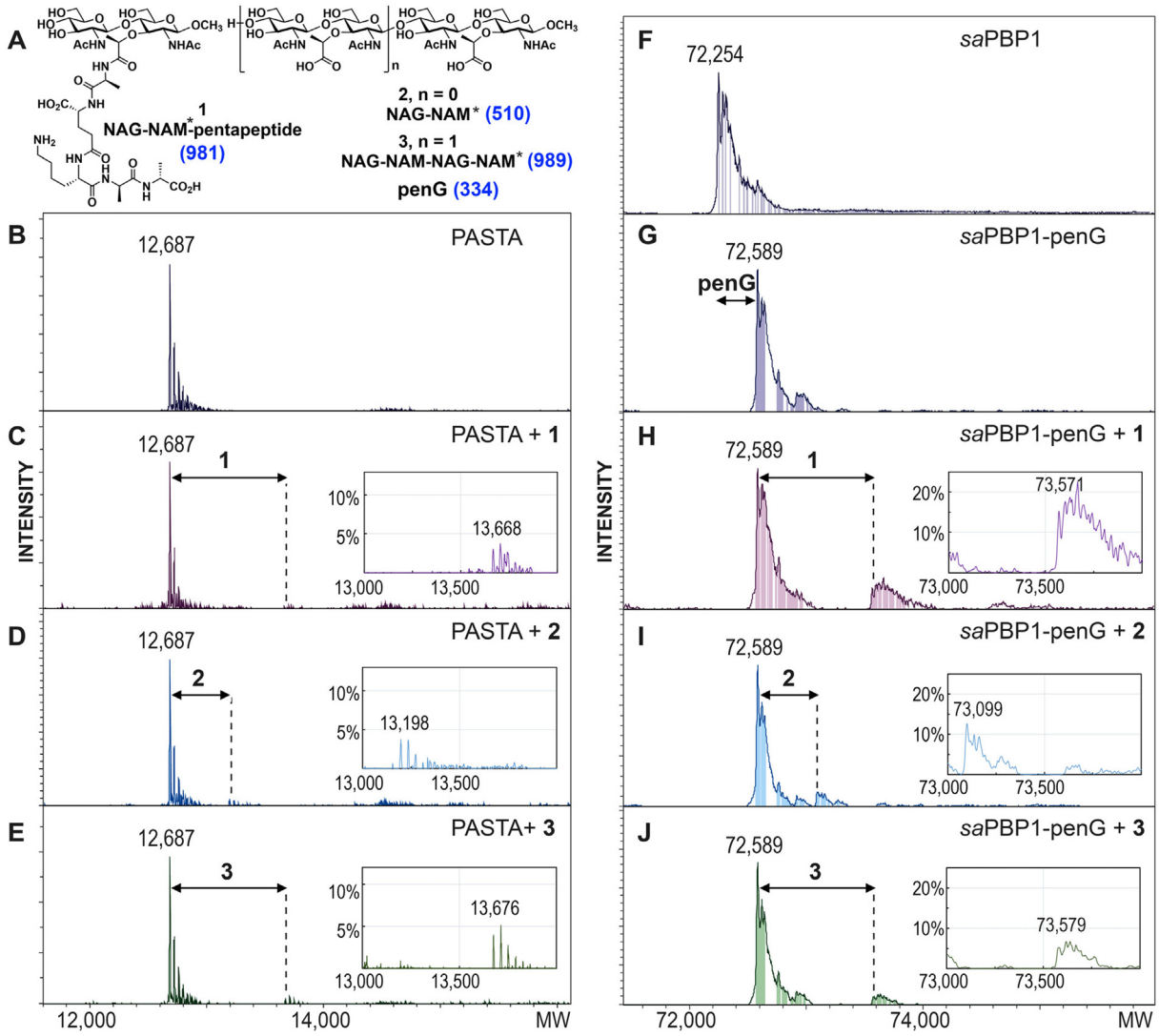

Fig. 4. Binding of synthetic peptidoglycans to the PASTA domains alone and to *sa*PBP1 with a blocked active site as a result of acylation by penicillin G (*sa*PBP1-penG) using non-denaturing mass spectrometry. (A) Chemical structures of synthetic peptidoglycans 1, 2, and 3 and their respective masses (blue text) are given. (B–E) The representative deconvoluted mass spectra of the PASTA domains alone (B), and in complex with 1 (C), 2 (D), and 3 (E). (F–J) The deconvoluted mass spectra of the *sa*PBP1 construct (F), *sa*PBP1-penG alone (G), and *sa*PBP1-PenG in complex with 1 (H), 2 (I), and 3 (J). The zoomed-in mass spectra are given as insets in panels C, D, E, H, I, and J. The mass spectra of proteins before PG binding are colored in dark gray (panels B, F, and G). The mass spectra of proteins in complexed with PGs are color coded per a specific PG – 1 in magenta, 2 in blue, and 3 in green. (For interpretation of the references to color in this figure legend, the reader is referred to the web version of this article.)

3.6. The saPBP1 structure inhibited by β-lactam acylation

The crystal structures of *sa*PBP1 in complex with piperacillin and penicillin G were solved at 3.03-Å and 2.59-Å resolution, respectively (Table 1). Both crystals have a different space group than the apo structure (two monomers in the asymmetric unit, Table 1). Overall, the two structures are not significantly different from the apo protein. Again, the PASTA domains were not visualized. The primary contrast was a poorly defined Loop 209–237 in the electron-density map (only some remnants of its density are seen at its *sa*PBP1 position). These structures underscore the mobility of the loop within the two extremes that are observed in the crystallographic apo structures. The most relevant main-chain alteration is the displacement (1.1 Å Cα atom of W351) of the β10 towards β11 (Lβ10–β11) connecting loop, in order to accommodate the acyl moiety attached to S314 by the antibiotics (Fig. 5A and 5B). Piperacillin acylation of S314 (Fig. 5A) is stabilized by van der Waals (W351, F423, I348, Y566, Y354) and polar interactions (S368, N370, T514, T516, Q425). Similar interactions are observed for penicillin G (Fig. 5B, but without contributions from N370 and T516). The carboxylate of the penicillin G acyl moiety ion pairs with the side chain of H499 (which reorients to establish this interaction: Figure S9). Small variations are also observed in the conformation of Q518 and N370 superimposing the *sa*PBP1-penicillin complex structures (Figure S9).

3.7. Substrate-binding cavities for the donor and acceptor peptidoglycan strands of saPBP1

The segment connecting α11 to β14 (in which H499 is found) and the helix α12 (in which Y566 residue is found) together generate strong differences in the expected trenches for the donor and acceptor strands (Figure S7C). For the transpeptidation reaction the *sa*PBP1 active site must accommodate two peptidoglycan strands. The donor strand acylates S314 to give an acyl-enzyme. Subsequent transfer of this acyl moiety to the acceptor strand crosslinks the peptidoglycan [71-73]. The donor-strand site of *sa*PBP1 is a large cavity, while the acceptor-strand site is a smal-

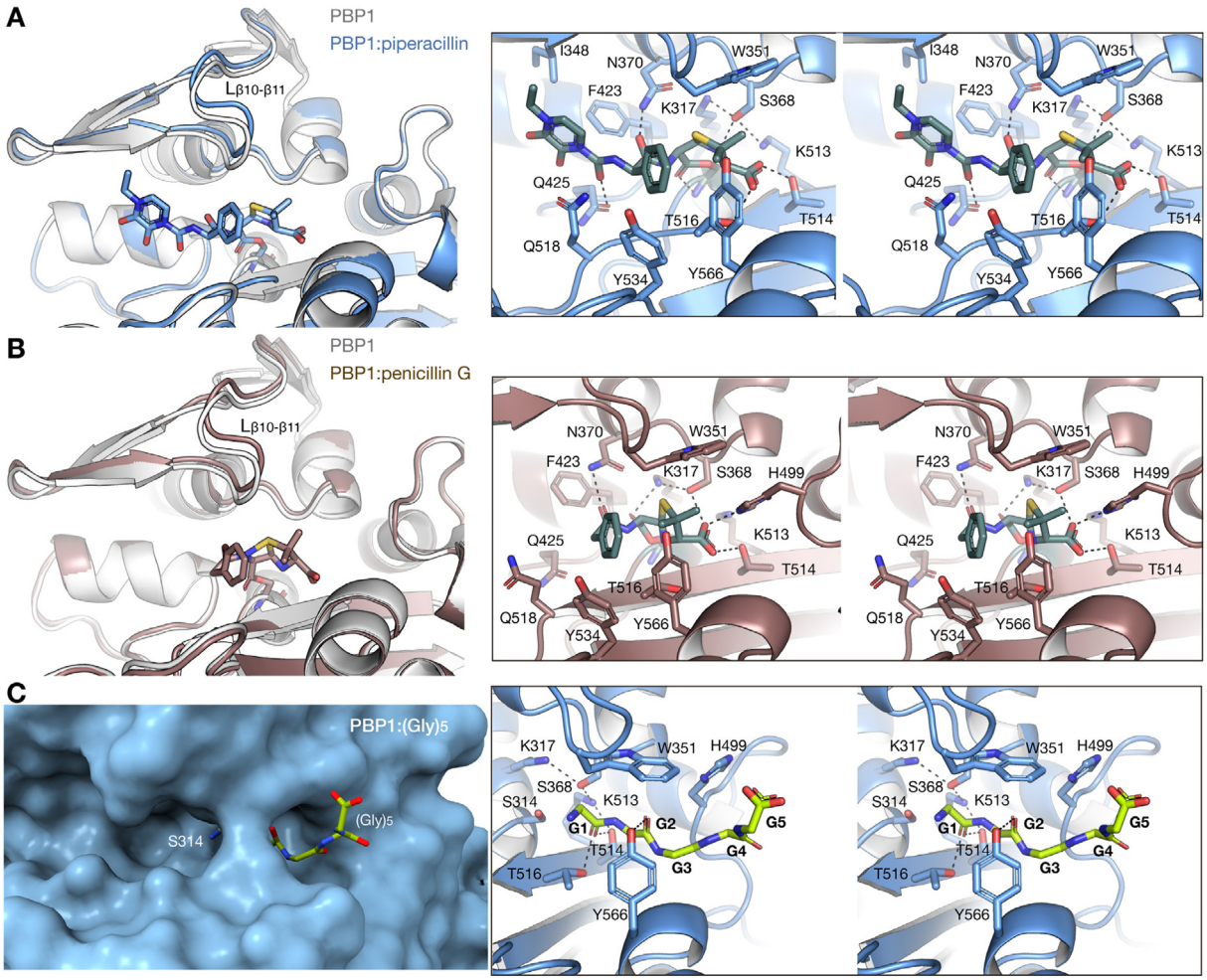

Fig. 5. Inhibition by β-lactams and the substrate occupancy at the acceptor site. (A) Structural superimposition of apo *sa*PBP1 (light gray ribbon) with the *sa*PBP1·piperacillin complex (blue ribbon) and (B) with the *sa*PBP1·penicillin G complex (brown ribbon). Boxed areas show stereo views of the relevant interactions between the protein and the antibiotics. (C) Three-dimensional structure of the *sa*PBP1:$(Gly)_5$ complex. Left, molecular surface of *sa*PBP1 at the active site with the pentaglycine strand represented as capped sticks colored by atom types (carbon in green). Right, stereo view of relevant interactions between acceptor peptide and *sa*PBP1. Polar interactions are represented as dotted lines. (For interpretation of the references to color in this figure legend, the reader is referred to the web version of this article.)

ler cavity (Figure S7A). This spatial arrangement conforms with the larger structure of the donor peptide compared to the narrower pentaglycyl structure (extending from the central lysine) of the acceptor strand (Fig. 1). The donor-strand site is occupied by the covalently-bound antibiotics in our *sa*PBP1:β-lactam complexes (Figure S7C). The acceptor-strand site was occupied by a molecule of HEPES buffer in our apo *sa*PBP1 (Fig. 2 and Figure S7C). Soaking the crystals with pentaglycine displaced the HEPES molecule and gave the crystal structure of the *sa*PBP1:$(Gly)_5$ complex, solved at 3.36-Å resolution (see methods and Table1). The pentaglycine is stabilized by polar and by van der Waals interactions (Fig. 5C). The carbonyl oxygen of the N-terminal Gly1 has hydrogen-bonding interactions with Thr514 and Thr516. Its terminal nitrogen atom points to the catalytic serine. Gly2 is hydrogen-bonded to the phenolic hydroxyl of Tyr566 (Fig. 5C). Besides these polar interactions with Gly1 and Gly2, the Gly1, Gly2, and Gly3 residues lining this narrow cavity have van der Waals interactions especially with Trp351, Tyr566, and His499. Interactions only with the first three Gly residues are observed (Fig. 5C).

Structural confirmation of a specific cavity for guiding the acceptor strand prompted comparison of PBP1 to the other *S. aureus* PBPs (the class A PBP2, PDB code 2OLU; the PBP2a·ceftaroline complex, PDB code 3ZFZ; and the PBP3:cefotaxime complex, PDB code 3VSL). Not surprisingly, the *S. aureus* PBPs show similarity for acceptor-strand recognition (Figure S10).

Whereas all PBPs from *S. aureus* show an acidic patch at the entrance of the acceptor-strand cavity, PBP1 shows the smallest one (Figure S10). The presence of this patch could be rationalized by the catalytic need for selection of the pentaglycyl moiety (with the cationic N-terminus of Gly1), to the exclusion of the carboxylate of the -D-Ala-D-Ala terminus of the donor-stem peptide. With this structural insight, we explored computationally the accommodation of two peptidoglycan strands on the PBP1 surface (Fig. 6A and Movie S5). Our model reveals a deep groove for the donor peptidoglycan (PG1 in Fig. 6A) and a shallow groove for the acceptor peptidoglycan (PG2 in Fig. 6A). The electrostatic surface potential for these grooves has acidic character for the recognition of glycan chains and basic character for the peptide stems of the peptidoglycan (Figure S11), as also observed with other peptidoglycan-binding proteins [45,74-76].

3.8. Computational modeling of PBP1:FtsW complex

Partnership of PBP1 and FtsW is essential to divisome function. The crystal structure of the homologous PBP2:RodA complex involved in elongation in the rod-shaped *Thermus thermophilus* led to the proposal that the PBP pedestal domain acts as an allos-

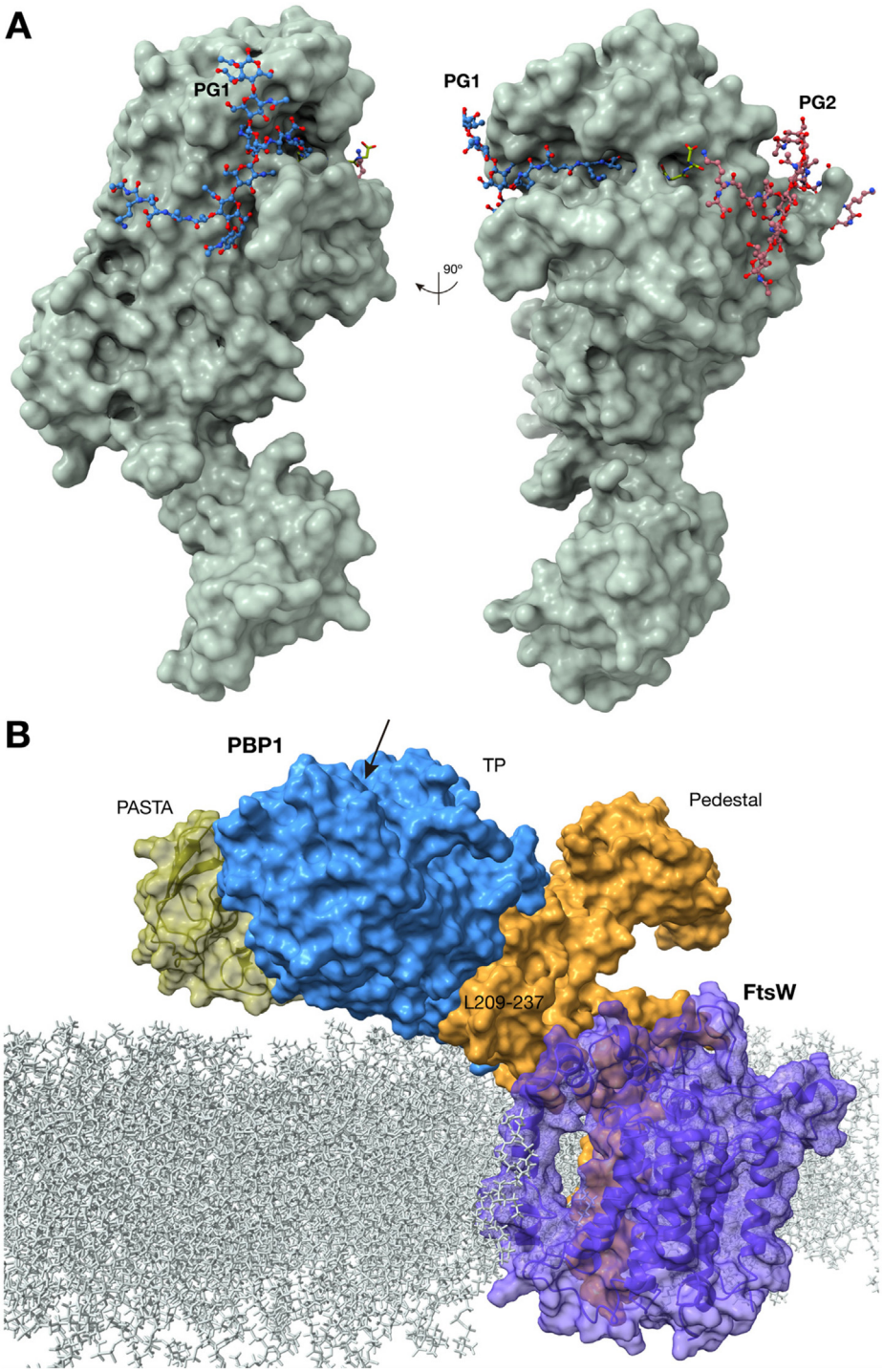

Fig. 6. Model for peptidoglycan binding to *sa*PBP1 and for the *sa*FtsW:*sa*PBP1 complex. (A) Model of donor and acceptor peptidoglycan strands attached to *sa*PBP1. Molecular-surface representation of *sa*PBP1 (green) in complex with pentaglycine (depicted with C atoms in green sticks). Modeled donor and acceptor strands are drawn as ball-and-sticks and colored in blue and pink, respectively. (B) Model of *sa*PBP1:*sa*FtsW complex based on PBP2:RodA complex (PDB code 6PL6). Molecular-surface representation of composite full-length *sa*PBP1 model (colored as in Fig. 2) and *sa*FtsW represented as transparent surface in magenta. Position of the active site of *sa*PBP1 is indicated by an arrow.

teric hub regulating and coordinating peptidoglycan biosynthesis [62]. The PBP2:RodA complex adopts an extended conformation (represented in the reported crystal structure) for Lipid II transglycosylase polymerization and a compact conformation for transpeptidase crosslinking of the peptidoglycan strands [62]. In the extended conformation interaction between the anchor subdomain (part of the pedestal domain) of PBP2 and the extracellular loop 4 (ECL4) of RodA (Figure S12A) would be responsible for activation of RodA. The equilibrium between the conformations was suggested to be regulated by MreC (or other proteins) of the elongasome complex [62]. This same regulation was proposed recently for the bPBP:SEDS complex of the divisome, despite the very different regulatory proteins of the divisome compared to the elongasome [77]. We explored this hypothesis by modeling the *sa*PBP1:*sa*FtsW complex of *S. aureus*, using the crystal structure of the *T. thermophilus* PBP2:RodA (PDB code 6PL6) as the template, in a lipid

bilayer membrane (Fig. 6B and S12B). *sa*FtsW has 10 transmembrane helices per secondary-structure prediction, and matches to *tt*RodA. In this model, the transmembrane anchor helix of *sa*PBP1 (not present in our crystal structure and thus modeled) interacts with *sa*FtsW (Figure S12B).

The conformation of L209–237 loop within the *sa*PBP1:*sa*FtsW complex is different from that of the cognate loop (L180-207) as observed in the *tt*PBP2:*tt*RodA complex (Figure S12). In the folded conformation (observed in our crystal structures, which also remained in a folded conformation during our 1-μs simulation; Movie S3), L209–237 could interact with other regions of *sa*FtsW or even with the membrane but the interaction with the ECL4 region of *sa*FtsW is unlikely to be enough to activate the SEDS protein (Fig. 6B and S12). Interestingly, the extended conformation that was observed in the *tt*PBP2:*tt*RodA complex would not permit the spatial location of the PASTA domains as observed in the *sp*PBP2x structure (if this conformation were to happen, the PASTA would insert into the membrane (Figure S12C). Therefore, the extended conformation for the *sa*PBP1:*sa*FtsW complex would imply movement of PASTA domains and detachment of the TP domain, in agreement with what we observed in *sa*PBP1 by X-ray crystallography, dynamics simulation and SAXS. The conformation of *sa*PBP1 with the folded L209–237 loop would then fit better with the compact conformation of the bPBP:SEDS complex in which the TP domain of PBP moves away from membrane to perform crosslinking of the newly synthetized peptidoglycan in proximity of the existing cell wall. Our structural complexes suggest how the peptidoglycan-donor and -acceptor strands are accommodated by *sa*PBP1 (Fig. 6A and Movie S5). In this report we have identified the spatial location of the PASTA domains in the *sa*PBP1 structure, demonstrated their mobility, and advanced the possibility of their involvement in cooperative recognition of peptidoglycan. These features suggest that the PASTA domains may have a role in directing the acceptor strand of peptidoglycan to the active site of PBP1. Further structural information is required to clarify the role of PASTA domains in regulation of cell-wall biosynthesis by the bPBP:SEDS complex during bacterial division.

4. Discussion

Our structural and modelling studies of *sa*PBP1 (65–713) allowed us, for the first time, to decipher the structural features and differences between *sa*PBP1 and other PBPs, in particular with its close structural homologue PBP2x. A relevant characteristic in *sa*PBP1 is the high mobility and flexibility of pedestal and PASTA domains, which was reflected in the absence of electronic density assignable for the PASTA domains from our X-ray data. We can conclude that the L209–237 loop in *sa*PBP1 is dynamic (as observed in the crystal structures) and that the PASTA domains preserve their compact fold, but are conformationally mobile and separated from the TP domain in contrast with the structures for its homologues PBP2x from *S. pneumoniae* and *S. thermophillus*. This motion is consistent with a role for the PASTA domains in the recognition of peptidoglycan and/or partner proteins within the divisome machinery. Our binding assays results suggest the participation of PASTA domains and the surface of *sa*PBP1 outside the active site for the recognition of peptidoglycan. While our structural (SAXS and X-ray crystallography) and molecular-dynamics results do not find evidence for a similar arrangement of PASTA and TP domains to that observed in *sp*PBP2x, our model of donor and acceptor peptidoglycan strands bound to *sa*PBP1 provide a plausible accommodation of the peptidoglycan near the active site (Fig. 5A). The binding is still observed although the interpretive limitation with respect to the weak binding towards *sa*PBP1 by the minimalist structure of the synthetic peptidoglycans. This occurs in contrast to the greater structural complexity of either the nascent or the mature peptidoglycan polymer, and the possibility of the other divisome proteins facilitating non-active-site peptidoglycan recognition by *sa*PBP1.

The momentous significance of the β-lactam antibiotics in the treatment of bacterial infection has driven decades of investigation addressing the structure and mechanism of the PBPs. The information in this report on *sa*PBP1 implements the information given by the known structures of the other four *S. aureus* PBPs. Not inconsequentially, *sa*PBP1 was the last of *S. aureus* PBPs for which structural knowledge was lacking. The exceptional clarity (1.51 Å resolution) of the structure of its PASTA domains will assist further study of their functional role. Reichmann et al. (2019) made the plausible suggestion that the PASTA domains are used to recognize a unique peptidoglycan structure created at mid-cell in the course of the early organization of the divisome [12]. Such a role is consistent with their mobility as suggested by molecular dynamics and seen by our crystallographic and SAXS analysis.

Regulation of the divisome machinery is complex and requires intervention of many different proteins in the process. Information about this question is of crucial relevance. Our results provide new insights into the complexity of this regulation and pave the way for the development of new compounds that can aid to prevent the expansion of the disease produced by this lethal human pathogen.

Declaration of Competing Interest

The authors declare that they have no known competing financial interests or personal relationships that could have appeared to influence the work reported in this paper.

Acknowledgments

The work in the USA was supported by grants AI104987 (to SM) and AI116548 (to MC) from the NIH. The work in Spain was funded by a grant from the Spanish Ministry of Science, Innovation and Competitiveness (BFU2017-90030-P and PID2020-115331GB-100 to JAH). We thank the staff from ALBA and Diamond Light Source synchrotrons for help during X-ray and SAXS data collection, respectively.

Author contributions

SM-C and RM determined crystal structures. KVM performed computational work. CK, RF and RB worked on protein production and functional characterization. ML and DH synthetized peptidoglycan analogues. ML performed non-denaturing mass spectrometry experiments. IM performed SAXS experiments and the requisite analysis. MC, SM and JAH led the respective collaborating groups and the overall project. All authors contributed to writing of the manuscript.

Appendix A. Supplementary data

Supplementary data to this article can be found online at https://doi.org/10.1016/j.csbj.2021.09.018.

References

[1] Caveney NA, Li FK, Strynadka NC. Enzyme structures of the bacterial peptidoglycan and wall teichoic acid biogenesis pathways. Curr Opin Struct Biol 2018;53:45–8. https://doi.org/10.1016/j.sbi.2018.05.002.
[2] Rajagopal M, Walker S. Envelope structures of gram-positive bacteria. Curr Top Microbiol Immunol 2017;404:1–44. https://doi.org/10.1007/82_2015_5021.
[3] Turner NA, Sharma-Kuinkel BK, Maskarinec SA, Eichenberger EM, Shah PP, Carugati M, et al. Methicillin-resistant Staphylococcus aureus: an overview of

basic and clinical research. Nat Rev Microbiol 2019;17:203–18. https://doi.org/10.1038/s41579-018-0147-4.
[4] Vollmer W, Blanot D, De Pedro MA. Peptidoglycan structure and architecture. FEMS Microbio Rev 2008;32:149–67. https://doi.org/10.1111/j.1574-6976.2007.00094.x.
[5] Vollmer W, Seligman SJ. Architecture of peptidoglycan: more data and more models. Trends Microbiol 2010;18:59–66. https://doi.org/10.1016/j.tim.2009.12.004.
[6] De Benedetti S, Fisher JF, Mobashery S. Practical Handbook of Microbiology. In: Practical Handbook of Microbiology. CRC Press; 2021. p. 167–204. https://doi.org/10.1201/9781003099277.
[7] Page JE, Walker S. Natural products that target the cell envelope. Curr Opin Microbiol 2021;61:16–24. https://doi.org/10.1016/j.mib.2021.02.001.
[8] Testero SA, Larrull LI, Fisher JF, Mobashery S. Medicinal Chemistry of ß-Lactam Antibiotics. Burgeŕs Medicinal Chemistry and Drug. Discovery 2021:1–188. https://doi.org/10.1002/0471266949.bmc226.pub2.
[9] Daitch AK, Goley ED. Uncovering unappreciated activities and niche functions of bacterial cell wall enzymes. Curr Biol 2020;30:R1170–5. https://doi.org/10.1016/j.cub.2020.07.004.
[10] Pinho MG, Filipe SR, De Lencastre H, Tomasz A. Complementation of the essential peptidoglycan transpeptidase function of penicillin-binding protein 2 (PBP2) by the drug resistance protein PBP2A in Staphylococcus aureus. J Bacteriol 2001;183:6525–31. https://doi.org/10.1128/JB.183.22.6525-6531.2001.
[11] Lund VA, Wacnik K, Turner RD, Cotterell BE, Walther CG, Fenn SJ, et al. Molecular coordination of Staphylococcus aureus cell division. ELife 2018;7. https://doi.org/10.7554/eLife.32057.
[12] Reichmann NT, Tavares AC, Saraiva BM, Jousselin A, Reed P, Pereira AR, et al. SEDS–bPBP pairs direct lateral and septal peptidoglycan synthesis in Staphylococcus aureus. Nat Microbiol 2019;4:1368–77. https://doi.org/10.1038/s41564-019-0437-2.
[13] Lakhundi S, Zhang K. Methicillin-resistant Staphylococcus aureus: molecular characterization, evolution, and epidemiology. Clin Microbiol Rev 2018;31. https://doi.org/10.1128/CMR.00020-18.
[14] Foster TJ. Can β-lactam antibiotics be resurrected to combat MRSA? Trends Microbiol 2019;27:26–38. https://doi.org/10.1016/j.tim.2018.06.005.
[15] Fisher JF, Mobashery S. Constructing and deconstructing the bacterial cell wall. Protein Sci 2020;29:629–46. https://doi.org/10.1002/pro.3737.
[16] Fisher JF, Mobashery S. β-Lactams against the Fortress of the Gram-Positive Staphylococcus aureus Bacterium. Chem Rev 2021;121:3612–13463. https://doi.org/10.1021/acs.chemrev.0c01010.
[17] Zhou X, Halladin DK, Rojas ER, Koslover EF, Lee TK, Huang KC, et al. Mechanical crack propagation drives millisecond daughter cell separation in Staphylococcus aureus. Science 2015;348:574–8.
[18] Saraiva BM, Sorg M, Pereira AR, Ferreira MJ, Caulat LC, Reichmann NT, et al. Reassessment of the distinctive geometry of Staphylococcus aureus cell division. Nature Commun 2020;11. https://doi.org/10.1038/s41467-020-17940-9.
[19] Pereira SFF, Henriques AO, Pinho MG, de Lencastre H, Tomasz A. Role of PBP1 in Cell Division of Staphylococcus aureus. J Bacteriol 2007;189:3525–31. https://doi.org/10.1128/JB.00044-07.
[20] Reed P, Atilano ML, Alves R, Hoiczyk E, Sher X, Reichmann NT, et al. Staphylococcus aureus survives with a minimal peptidoglycan synthesis machine but sacrifices virulence and antibiotic resistance. PLoS Pathog 2015;11. https://doi.org/10.1371/journal.ppat.1004891.
[21] Monteiro JM, Pereira AR, Reichmann NT, Saraiva BM, Fernandes PB, Veiga H, et al. Peptidoglycan synthesis drives an FtsZ-treadmilling-independent step of cytokinesis. Nature 2018;554:528–32. https://doi.org/10.1038/nature25506.
[22] Straume D, Piechowiak KW, Kjos M, Håvarstein LS. Class A PBPs: It is time to rethink traditional paradigms. Mol Microbiol 2021. https://doi.org/10.1111/mmi.14714.
[23] Lovering AL, De Castro LH, Lim D, Strynadka NCJ. Structural insight into the transglycosylation step of bacterial cell-wall biosynthesis. Science 2007;315:1402–5. https://doi.org/10.1126/science.1136611.
[24] Welsh MA, Schaefer K, Taguchi A, Kahne D, Walker S. Direction of chain growth and substrate preferences of shape, elongation, division, and sporulation-family peptidoglycan glycosyltransferases. J Am Chem Soc 2019;141:12994–7. https://doi.org/10.1021/jacs.9b06358.
[25] Egan AJF, Errington J, Vollmer W. Regulation of peptidoglycan synthesis and remodelling. Nat Rev Microbiol 2020;18:446–60. https://doi.org/10.1038/s41579-020-0366-3.
[26] Yeats C, Finn RD, Bateman A. The PASTA domain: A β-lactam-binding domain. Trends Biochem Sci 2002;27:438–40. https://doi.org/10.1016/S0968-0004(02)02164-3.
[27] Calvanese L, Falcigno L, Squeglia F, D'auria G, Berisio R. Structural and dynamic features of PASTA domains with different functional roles. J Biomol Struct Dyn 2017;35:2293–300. https://doi.org/10.1080/07391102.2016.1217274.
[28] Pensinger DA, Schaenzer AJ, Sauer JD. Do shoot the messenger: PASTA kinases as virulence determinants and antibiotic targets. Trends Microbiol 2018;26:56–69. https://doi.org/10.1016/j.tim.2017.06.010.
[29] Djorić D, Minton NE, Kristich CJ. The enterococcal PASTA kinase: a sentinel for cell envelope stress. Mol Oral Microbiol 2021;36:132–44. https://doi.org/10.1111/omi.12313.
[30] Pares S, Mouz N, Pétillot Y, Hakenbeck R, Dideberg O. X-ray structure of Streptococcus pneumoniae PBP2x, a primary penicillin target enzyme. Nat Struct Biol 1996;3:284–9. https://doi.org/10.1038/nsb0396-284.
[31] Barthe P, Mukamolova GV, Roumestand C, Cohen-Gonsaud M. The structure of PknB extracellular PASTA domain from mycobacterium tuberculosis suggests a ligand-dependent kinase activation. Structure 2010;18:606–15. https://doi.org/10.1016/j.str.2010.02.013.
[32] Paracuellos P, Ballandras A, Robert X, Kahn R, Hervé M, Mengin-Lecreulx D, et al. The extended conformation of the 2.9-Å Crystal Structure of the Three-PASTA Domain of a Ser/Thr kinase from the human pathogen Staphylococcus aureus. J Mol Biol 2010;404:847–58. https://doi.org/10.1016/j.jmb.2010.10.012.
[33] Ruggiero A, Squeglia F, Marasco D, Marchetti R, Molinaro A, Berisio R. X-ray structural studies of the entire extracellular region of the serine/threonine kinase PrkC from Staphylococcus aureus. Biochem J 2011;435:33–41. https://doi.org/10.1042/BJ20101643.
[34] Calvanese L, Falcigno L, Maglione C, Marasco D, Ruggiero A, Squeglia F, et al. Structural and binding properties of the PASTA domain of PonA2, a key penicillin binding protein from Mycobacterium tuberculosis. Biopolymers 2014;101:712–9. https://doi.org/10.1002/bip.22447.
[35] Angeles DM, Macia-Valero A, Bohorquez LC, Scheffers DJ. The pasta domains of bacillus subtilis PBP2B strengthen the interaction of PBP2B with DIVIB. Microbiology (United Kingdom) 2020;166:826–36. https://doi.org/10.1099/mic.0.000957.
[36] Righino B, Galisson F, Pirolli D, Vitale S, Réty S, Gouet P, et al. Structural model of the full-length Ser/Thr protein kinase StkP from S. pneumoniae and its recognition of peptidoglycan fragments. J Biomol Struct Dyn 2017;1102:1–14. https://doi.org/10.1080/07391102.2017.1395767.
[37] Wamp S, Rutter ZJ, Rismondo J, Jennings CE, Möller L, Lewis RJ, et al. Prka controls peptidoglycan biosynthesis through the essential phosphorylation of ReoM. ELife 2020;9:1–75. https://doi.org/10.7554/eLife.56048.
[38] Bernardo-García N, Mahasenan KV, Batuecas MT, Lee M, Hesek D, Petráčková D, et al. Allostery, recognition of nascent peptidoglycan, and cross-linking of the cell wall by the essential penicillin-binding protein 2x of Streptococcus pneumoniae. ACS Chem Biol 2018;13:694–702. https://doi.org/10.1021/acschembio.7b00817.
[39] Zucchini L, Mercy C, Garcia PS, Cluzel C, Gueguen-Chaignon V, Galisson F, et al. PASTA repeats of the protein kinase StkP interconnect cell constriction and separation of Streptococcus pneumoniae. Nat Microbiol 2018;3:197–209. https://doi.org/10.1038/s41564-017-0069-3.
[40] Yoshida H, Kawai F, Obayashi E, Akashi S, Roper DI, Tame JRH, et al. Crystal structures of penicillin-binding protein 3 (PBP3) from methicillin-resistant staphylococcus aureus in the Apo and cefotaxime-bound forms. J Mol Biol 2012;423:351–64. https://doi.org/10.1016/j.jmb.2012.07.012.
[41] Navratna V, Nadig S, Sood V, Prasad K, Arakere G, Gopal B. Molecular basis for the role of Staphylococcus aureus penicillin binding protein 4 in antimicrobial resistance. J Bacteriol 2010;192:134–44. https://doi.org/10.1128/JB.00822-09.
[42] Mahasenan KV, Molina R, Bouley R, Batuecas MT, Fisher JF, Hermoso JA, et al. Conformational dynamics in penicillin-binding protein 2a of methicillin-resistant staphylococcus aureus, allosteric communication network and enablement of catalysis. J Am Chem Soc 2017;139:2102–10. https://doi.org/10.1021/jacs.6b12565.
[43] Alexander JAN, Chatterjee SS, Hamilton SM, Eltis LD, Chambers HF, Strynadka NCJ. Structural and kinetic analyses of penicillin-binding protein 4 (PBP4)-mediated antibiotic resistance in Staphylococcus aureus. J Biol Chem 2018;293:19854–65. https://doi.org/10.1074/jbc.RA118.004952.
[44] Hesek D, Suvorov M, Morio KI, Lee M, Brown S, Vakulenko SB, et al. Synthetic peptidoglycan substrates for penicillin-binding protein 5 of gram-negative bacteria. J Org Chem 2004;69:778–84. https://doi.org/10.1021/jo035397e.
[45] Martínez-Caballero S, Lee M, Artola-Recolons C, Carrasco-López C, Hesek D, Spink E, et al. Reaction products and the X-ray structure of AmpDh2, a virulence determinant of Pseudomonas aeruginosa. J Am Chem Soc 2013;135:10318–21. https://doi.org/10.1021/ja405464b.
[46] Lee M, Hesek D, Dik DA, Fishovitz J, Lastochkin E, Boggess B, et al. From genome to proteome to elucidation of reactions for all eleven known lytic transglycosylases from pseudomonas aeruginosa. Angew Chem 2017;129:2779–83. https://doi.org/10.1002/ange.201611279.
[47] Hernández H, Robinson CV. Determining the stoichiometry and interactions of macromolecular assemblies from mass spectrometry. Nat Protoc 2007;2:715–26. https://doi.org/10.1038/nprot.2007.73.
[48] Alcorlo M, Dik DA, De Benedetti S, Mahasenan KV, Lee M, Domínguez-Gil T, et al. Structural basis of denuded glycan recognition by SPOR domains in bacterial cell division. Nat Commun 2019;10:1–13. https://doi.org/10.1038/s41467-019-13354-4.
[49] Xds KW. Acta Crystallogr D Biol Crystallogr 2010;66:125–32. https://doi.org/10.1107/S0907444909047337.
[50] Evans PR, Murshudov GN. How good are my data and what is the resolution? Acta Crystallogr D Biol Crystallogr 2013;69:1204–14. https://doi.org/10.1107/S0907444913000061.
[51] Tickle IJ, Flensburg C, Keller P, Paciorek W, Sharff A, Vonrhein C, et al. STARANISO 2018.
[52] Vonrhein C, Flensburg C, Keller P, Sharff A, Smart O, Paciorek W, et al. Data processing and analysis with the autoPROC toolbox. Acta Crystallogr D Biol Crystallogr 2011;67:293–302. https://doi.org/10.1107/S0907444911007773.
[53] Vagin A, Teplyakov A. Molecular replacement with MOLREP. Acta Crystallogr D Biol Crystallogr 2010;66:22–5. https://doi.org/10.1107/S0907444909042589.
[54] Afonine PV, Grosse-Kunstleve RW, Echols N, Headd JJ, Moriarty NW, Mustyakimov M, et al. Towards automated crystallographic structure refinement with phenix.refine. Acta Crystallogr D Biol Crystallogr 2012;68:352–67. https://doi.org/10.1107/S0907444912001308.

[55] Murshudov GN, Vagin AA, Dodson EJ. Refinement of macromolecular structures by the maximum-likelihood method. Acta Crystallogr D Biol Crystallogr 1997;53:240–55. https://doi.org/10.1107/S0907444996012255.
[56] Emsley P, Lohkamp B, Scott WG, Cowtan K. Features and development of Coot. Acta Crystallogr D Biol Crystallogr 2010;66:486–501. https://doi.org/10.1107/S0907444910007493.
[57] Winn MD, Ballard CC, Cowtan KD, Dodson EJ, Emsley P, Evans PR, et al. Overview of the CCP4 suite and current developments. Acta Crystallogr D Biol Crystallogr 2011;67:235–42. https://doi.org/10.1107/S0907444910045749.
[58] McCoy AJ, Grosse-Kunstleve RW, Adams PD, Winn MD, Storoni LC, Read RJ. Phaser crystallographic software. J Appl Crystallogr 2007;40:658–74. https://doi.org/10.1107/S0021889807021206.
[59] Pierce BG, Hourai Y, Weng Z. Accelerating protein docking in ZDOCK using an advanced 3D convolution library. PLoS ONE 2011;6. https://doi.org/10.1371/journal.pone.0024657.
[60] Pierce BG, Wiehe K, Hwang H, Kim BH, Vreven T, Weng Z. ZDOCK server: interactive docking prediction of protein-protein complexes and symmetric multimers. Bioinformatics 2014;30:1771–3. https://doi.org/10.1093/bioinformatics/btu097.
[61] Case DA, Ben-Shalom IY, Brozell SR, Cerutti D, Cheatham III TE, Cruzeiro VWD, et al. AMBER 18 2018.
[62] Sjodt M, Rohs PDA, Gilman MSA, Erlandson SC, Zheng S, Green AG, et al. Structural coordination of polymerization and crosslinking by a SEDS–bPBP peptidoglycan synthase complex. Nat Microbiol 2020;5:813–20. https://doi.org/10.1038/s41564-020-0687-z.
[63] Cowieson NP, Edwards-Gayle CJC, Inoue K, Khunti NS, Doutch J, Williams E, et al. Beamline B21: high-throughput small-angle X-ray scattering at Diamond Light Source. J Synchrotron Radiat 2020;27:1438–46. https://doi.org/10.1107/S1600577520009960.
[64] Petoukhov MV, Franke D, Shkumatov AV, Tria G, Kikhney AG, Gajda M, et al. New developments in the ATSAS program package for small-angle scattering data analysis. J Appl Crystallogr 2012;45:342–50. https://doi.org/10.1107/S0021889812007662.
[65] Schneidman-Duhovny D, Hammel M, Tainer JA, Sali A. FoXS, FoXSDock and MultiFoXS: single-state and multi-state structural modeling of proteins and their complexes based on SAXS profiles. Nucleic Acids Res 2016;44:W424–9. https://doi.org/10.1093/nar/gkw389.
[66] Gordon E, Mouz N, Duée E, Dideberg O. The crystal structure of the penicillin-binding protein 2x from Streptococcus pneumoniae and its acyl-enzyme form: implication in drug resistance. J Mol Biol 2000;299:477–85. https://doi.org/10.1006/jmbi.2000.3740.
[67] Adediran SA, Sarkar KS, Pratt RF. Kinetic evidence for a second ligand binding site on Streptococcus pneumoniae penicillin-binding protein 2x. Biochemistry 2018;57:1758–66. https://doi.org/10.1021/acs.biochem.7b01209.
[68] Hamelberg D, Mongan J, McCammon JA. Accelerated molecular dynamics: a promising and efficient simulation method for biomolecules. J Chem Phys 2004;120:11919–29. https://doi.org/10.1063/1.1755656.
[69] Maestro B, Novaková L, Hesek D, Lee M, Leyva E, Mobashery S, et al. Recognition of peptidoglycan and β-lactam antibiotics by the extracellular domain of the Ser/Thr protein kinase StkP from Streptococcus pneumoniae. FEBS Lett 2011;585:357–63. https://doi.org/10.1016/j.febslet.2010.12.016.
[70] Squeglia F, Marchetti R, Ruggiero A, Lanzetta R, Marasco D, Dworkin J, et al. Chemical basis of peptidoglycan discrimination by PrkC, a key kinase involved in bacterial resuscitation from dormancy. J Am Chem Soc 2011;133:20676–9. https://doi.org/10.1021/ja208080r.
[71] Macheboeuf P, Contreras-Martel C, Job V, Dideberg O, Andŕ A, Dessen A. Penicillin Binding Proteins: key players in bacterial cell cycle and drug resistance processes. FEMS Microbiol Rev 2006;30:673–91. https://doi.org/10.1111/j.1574-6976.2006.00024.x.
[72] Srisuknimit V, Qiao Y, Schaefer K, Kahne D, Walker S. Peptidoglycan cross-linking preferences of Staphylococcus aureus penicillin-binding proteins have implications for treating MRSA infections. J Am Chem Soc 2017;139:9791–4. https://doi.org/10.1021/jacs.7b04881.
[73] Shi Q, Meroueh SO, Fisher JF, Mobashery S. A computational evaluation of the mechanism of penicillin-binding protein-catalyzed cross-linking of the bacterial cell wall. J Am Chem Soc 2011;133:5274–83. https://doi.org/10.1021/ja1074739.
[74] Lee M, Artola-Recolons C, Carrasco-López C, Martínez-Caballero S, Hesek D, Spink E, et al. Cell-wall remodeling by the zinc-protease AmpDh3 from pseudomonas aeruginosa. J Am Chem Soc 2013;135:12604–7. https://doi.org/10.1021/ja407445x.
[75] Artola-Recolons C, Lee M, Bernardo-García N, Blázquez B, Hesek D, Bartual SG, et al. Structure and cell wall cleavage by modular lytic transglycosylase MltC of Escherichia coli. ACS Chem Biol 2014;9:2058–66. https://doi.org/10.1021/cb500439c.
[76] Lee M, Batuecas MT, Tomoshige S, Domínguez-Gil T, Mahasenan KV, Dik DA, et al. Exolytic and endolytic turnover of peptidoglycan by lytic transglycosylase Slt of Pseudomonas aeruginosa. PNAS 2018;115:4393–8. https://doi.org/10.1073/pnas.1801298115.
[77] Li Y, Gong H, Zhan R, Ouyang S, Park K-T, Lutkenhaus J, et al. Genetic analysis of the septal peptidoglycan synthase FtsWI complex supports a conserved activation mechanism for SEDS-bPBP complexes. PLoS Genet 2021;17:. https://doi.org/10.1371/journal.pgen.1009366e1009366.